JACS
JOURNAL OF THE AMERICAN CHEMICAL SOCIETY
Article
pubs.acs.org/JACS

A Gold Nanoparticle Pentapeptide: Gene Fusion To Induce Therapeutic Gene Expression in Mesenchymal Stem Cells

Megan E. Muroski,[†,§] Thomas J. Morgan, Jr.,[‡,§] Cathy W. Levenson,[‡] and Geoffrey F. Strouse*[,†,‡]

[†]Department of Chemistry and Biochemistry, 95 Chieftan Way, Florida State University, Tallahassee, Florida 32306-4390, United States

[‡]College of Medicine, 1115 West Call Street, Florida State University, Tallahassee, Florida 32306-4300, United States

Supporting Information

ABSTRACT: Mesenchymal stem cells (MSC) have been identified as having great potential as autologous cell therapeutics to treat traumatic brain injury and spinal injury as well as neuronal and cardiac ischemic events. All future clinical applications of MSC cell therapies must allow the MSC to be harvested, transfected, and induced to express a desired protein or selection of proteins to have medical benefit. For the full potential of MSC cell therapy to be realized, it is desirable to systematically alter the protein expression of therapeutically beneficial biomolecules in harvested MSC cells with high fidelity in a single transfection event. We have developed a delivery platform on the basis of the use of a solid gold nanoparticle that has been surface modified to produce a fusion containing a zwitterionic, pentapeptide designed from Bax inhibiting peptide (Ku70) to enhance cellular uptake and a linearized expression vector to induce enhanced expression of brain-derived neurotrophic factor (BDNF) in rat-derived MSCs. Ku70 is observed to effect >80% transfection following a single treatment of femur bone marrow isolated rat MSCs with efficiencies for the delivery of a 6.6 kbp gene on either a Au nanoparticle (NP) or CdSe/ZnS quantum dot (QD). Gene expression is observed within 4 d by optical measurements, and secretion is observed within 10 d by Western Blot analysis. The combination of being able to selectively engineer the NP, to colocalize biological agents, and to enhance the stability of those agents has provided the strong impetus to utilize this novel class of materials to engineer primary MSCs.

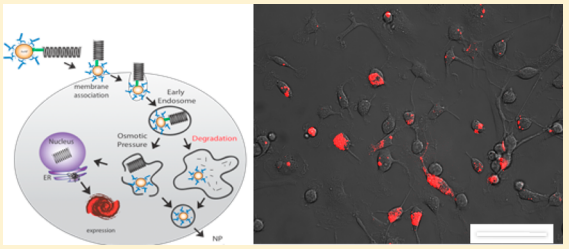

The desire to develop biomedical approaches to personalize medicine has led to the expressed goal of manipulating one's own cells to intentionally alter the cell function for therapeutic applications.[1−3] Stem cell therapy approaches represent an important cell therapy technology that is already being realized for treatment of stroke, traumatic brain injury, neurodegenerative diseases, cardiac, and spinal injuries.[4−12] Bone marrow derived mesenchymal stem cells (MSCs) are advantageous for cell therapy applications as they lack immune response, have inherent pluripotency, exhibit natural transport to sites of injury, and display reparative properties.[6,9,13−15] The use of stem cells offers an approach to realize the goals of personalized medicine if the stem cell can be routinely and selectively engineered to express therapeutic proteins targeting specific disease states. The ability to genetically manipulate stem cells using a routine approach that does not elicit cell death offers unprecedented opportunities to expand the therapeutic benefit of a patient's own cells to conquer disease and potentially to realize personalized medicine.

Whether the goal is to isolate a stem cell patch to repair disease-related damage in an individual or to use the cell to express and deliver therapeutic proteins to a site of injury, the ability to selectively engineer a stem cell to act as a therapeutic bioreactor could broaden the applicability of cell therapy. Patient-derived and donor stem cells both offer potential therapeutic cell lines that can be selectively engineered. Of the exogenous stem cells, MSCs are ideal candidates for cell therapy applications. Unfortunately, MSCs can be difficult to transfect without impacting the pluripotency or cell viability and often result in poor efficiencies;[16−18] thus, clinical studies have been largely limited to unmodified lines.[4,19−21]

While transforming immortalized cells today is considered routine via nonviral strategies, MSC transfection is not.[1,2,22−27] Stem cells are known to be resistant to genetic manipulation with the few successful genetically modified lines produced using inefficient electroporation methods (40% Nucleofector) or very efficient viral vectors (80%).[28−31] Electroporation is known to be efficient but with significant loss of viable cells with <50% viable following treatment. Viral vectors, wherein a desired gene is repackaged into a viral capsid, while efficient are expensive, have substantial biosafety restrictions, and pose a significant risk of secondary infection and immunogenic response.[32−37] Alternative transfection approaches including polymeric agents and lipid agents as carriers of bimolecular payloads have been unpredictable and often not highly efficient (25% PEI, 2−35% cationic liposomes) for MSC transfection without loss of viability.[38−43] Such nonviral approaches are based upon encapsulation in a cationic polyplex (Lipofectamine, PEI, JetPrime, etc.) and routinely exhibit low single

Received: May 23, 2014
Published: September 8, 2014

   dx.doi.org/10.1021/ja505190q | J. Am. Chem. Soc. 2014, 136, 14763−14771

passage efficiency, require extensive optimization, and are cytotoxic because of the chemical composition of the agent.[1,25,26,44,45] The difficulty to transfect MSCs stems from the variability in the cell population and the toxicity of many of the transfection methods.

New nonviral approaches that might improve MSC engineering are being explored including the use of nanoparticle transport complexes (NP-complex) containing appended gene regulatory elements that are released passively following endosomal uptake of the NP-complex.[46] While the NP can be formed from a myriad of core particles, gold nanoparticles (AuNP) are by far recognized as the most promising nanoparticle agent being nontoxic and easily modified by a gene, RNA, short DNA sequences, or a combination of the agents on a single nanoparticle carrier.[46−61] 61 Early studies using combinations of gene regulatory elements coassembled onto a AuNP-complex were effective in regulating protein expression when encapsulated in commercial lipids.[46]

In a growing set of studies, the use of cell-penetrating peptides (CPP) has been shown to be more effective for enhancing cellular uptake of the NP-complexes and for eliminating cytotoxicity of the lipid.[62−70] The use of highly charged arginine rich peptides (HIV-TAT, Penatrin, VP-22) is reported to improve uptake and is rapidly being exploited in the nanoparticle-assisted transfection field. On nanoparticles, the highly charged viral protein coats may enhance transfection, but the high surface charge leads to nonspecific electrostatic packaging of the phosphate backbone of a delivered gene.[71]

To avoid the effects of electrostatic interactions but to still take advantage of the enhanced transfection efficiencies when a CPP is used, a neutral CPP would be ideal. In the transfection literature, a novel class of short peptides has been identified as transfection enhancers that exhibit low charge.[72] While their mechanism for cellular uptake is not known, the limited studies suggest that efficient package delivery can be achieved through use of simple peptide sequences that are in effect zwitterionic or net neutral when bound to a nanoparticle surface.[64] Of the short peptide sequences known, the Bax inhibiting peptide is an intriguing pentapeptide derived from Ku70 that has shown promising results in preliminary transfection studies when appended to the c-terminus of GFP. Ku70 is a DNA binding sequence involved in DNA repair and is thought to play a role in antiapoptosis. The coupling of a cysteine to the N-terminus of the Ku70 pentapeptide makes the peptide sequence zwitterionic and ideal for application as a transfection enhance for gene delivery on a nanoparticle carrier; cytotoxicity complications often arise for charged peptide sequences or secondary transfection agents. More importantly, the use of Ku70 to enhance gene delivery on a nanoparticle can open new directions in nonviral genetic engineering of cell lines with potential clinical applications for cell therapeutics. To date, there are no reported studies of using Ku70 to enhance nanoparticle uptake when a gene is coassembled onto the nanoparticle surface for genetic engineering applications.

In this manuscript, the modification of a set of nanoparticles (6.6 nm Au and a 6.0 nm CdSe/ZnS, by a N-terminal cysteine modified Ku70 neutral peptide) is demonstrated to be an effective transfection of rMSCs of brain-derived neurotrophic factor (BDNF)/mCherry fusion gene (6.6 kbp) delivered on a AuNP and the quantum dot (QD) without the gene. While the chemistry of the QD and AuNP is unique in a cell, the observation of efficient uptake of these particles into rMSCs by using the Ku70 peptide is important. Because of the biomedical potential of AuNPs, the study focuses on the results of transfection by the AuNP; the Ku70 modified AuNP is comodified through thiol linkage chemistry to deliver a 6.6 kbp gene designed to express a secreted BDNF/mCherry fusion protein. The coassembly of the peptide and the gene is in a 500:1 mol ratio. The 6.6kb gene is a linearized construct containing a synthetic linker sequence with a C_6-thiol appendage for coupling to the NP surface and a cytomegalovirus (CMV) promoter for overexpression of the fusion protein BDNF/mCherry. The studies on the Ku70 modified 6.0 nm CdSe/ZnS and superparamagnetic iron oxide (SPIO) particle are only used to demonstrate uptake potential of nanoparticles when modified by the Bax inhibiting protein pentapeptide.

Following a single challenge of the MSCs by the NP-complexes, efficient cellular uptake of the NP package with ∼80% cell transfection is observed for the delivered nanoparticles (80% AuNP-gene construct and 82% CdSe/ZnS). The genetically modified MSCs exposed to a single transfection by the AuNP-gene construct exhibit subsequent protein expression of a secreting BDNF/mCherry fusion protein, which can be observed by optical microscopy early in the cell cycle (within 4 d), and the rise in BDNF in the media is measured by Western blot analysis of tetrachloroacetic acid (TCA) precipitated media (within 10 d) as the protein levels increase in the media. We observe exogenous protein expression of BDNF/mCherry, no changes in viability for >2 weeks (93.8%), and no effect on a panel of limited antibody markers for stemness (CD-90, CD-54, and CD-45).

The results indicate that the use of N-cysteine modified Ku70 peptides is effective at cell transfection, providing an NP transfection strategy that has the advantage of avoiding the viral gene transfer technology while maintaining the power of being able to effectively deliver a gene up to 6.6 kbp of choice. The demonstration of the ability to routinely transfect a primary MSC culture by a large plasmid (6.6 kbp) using a nonviral vector in a single-step treatment is an important step forward for developing methods for routine MSC engineering.

METHODS

UV−Vis. The AuNP-complex is analyzed by UV−vis absorption spectroscopy on a Cary Eclipse by monitoring the AuNP surface plasmon resonance at 540 nm compared to the 280 nm peptide and 260 nm gene absorption features. The ratio of gene to peptide to AuNP is assessed using the extinction coefficients of the components to estimate the loading ratios of the individual components. To ensure the AuNP absorption does not impact the peptide and DNA absorption features, the AuNP-complex is treated with 0.5 mM NaCN to dissolve the AuNP allowing direct analysis of the gene-to-peptide ratios.[73] The dissolution of the AuNP was allowed to occur at room temperature (RT) for 5 min. Control studies were carried out on single component appended AuNP-complexes for comparison. The digestion studies were conducted in triplicate. Experimental details for cyanide digestion are available in the Supporting Information.

Dynamic Light Scattering. The hydrodynamic radii of the AuNP-complexes and controls were analyzed using dynamic light scattering (DLS) performed on a DynaPro Titan DLS system (Wyatt Technologies, Santa Barbara) at 20% laser power (830 nm) for complexes resuspended in deionized (DI) water. The hydrodynamic radius is calculated by averaging 20 measurements with an acquisition time of 1 s.

Optical Microscopy. Wide-field microscopy images were collected on an inverted Nikon TE2000-E2 Eclipse C1si (Nikon Instruments Inc., U.S.) following transfection by the AuNP-chimera. Experiments were conducted in triplicate. The optical imaging was carried out in 10

cm^2 optical dishes using DMEM7777 media on cells plated at 30 000 cell/cm^2 using a microscope live-cell chamber (Pathology devices, LiveCell 5% CO_2, 50% humidity). Fluorescence images were acquired with a CFI Plan Apochromat 40× objective (NA 0.95, 0.14 mm WD), 5.49 electronic zoom. The samples were imaged with a Cool SNAP HQ2 monochrome camera (Photometric) and were analyzed with Nikon NIS Elements software. The samples were excited using a white light metal halide source, and the emission was monitored in the Texas Red filter cube for monitoring mCherry emission.

Western Blot Analysis. A semiquantitative, time-dependent Western Blot analysis was carried out in order to measure the increasing level of secreted mCherry and BDNF levels in media. The reported BDNF concentrations were relative to pretransfection BDNF levels by ensuring that identical concentrations of media were screened. The Western blot data were measured on equal volumes of media removed from the MSC cultures (six well dishes, Nunc) and were measured relative to a control (untransfected). The media proteins were precipitated with 1/100 volume of 2% deoxycholate for 1 h on ice followed by addition of 1/10 volume of 100% trichloroacetic acid overnight at 4 °C. Pellets that formed were washed three times in ice-cold acetone, and then the samples (n = 3/condition) were subjected to sodium dodecyl sulfate polyacrylamide gel electrophoresis using a 4−20% polyacrylamide gel and then were transferred to a 0.2 μm nitrocellulose membrane. The membrane was blocked with Superblock T20 (Thermo Scientific) for 1 h at room temperature followed by an overnight incubation with a rabbit polyclonal antibody to BDNF (sc 546 Santa Cruz) or with a mouse monoclonal antibody to red fluorescent protein (akr-021 Cell Biolabs) for mCherry. Membranes were then washed and incubated with the corresponding IRDye goat antirabbit (680LT) or IRDye goat antimouse (800 CW, LI-COR Biosciences) secondary antibodies in Superblock. Immunoreactive bands were visualized using the Odyssey infrared detection method with corresponding software (LI-COR Bioscience, NE, U.S.).

Rat Mesenchymal Stem Cells (rMSC). Primary rMSCs were harvested from bone marrow extracted from rat femurs using the method of Nadri et al.[74] Briefly, the bone marrow was extracted by flushing with Dulbecco's modified Eagle's medium (DMEM, D7777 Sigma) using a 22G needle and collecting the bone marrow into 50 mL sterile conical tubes. The marrow extract was filtered through a 70 μm cell strainer and was pelleted at 1500 rpm for 3 min. The cell pellet was resuspended in 15 mL of DMEM containing 10% fetal bovine serum (FBS) (HyClone) and 1% Pen-Strep and was seeded into a T-75 cm^2 flask and was maintained at 37 °C and 5% CO_2 with the medium changed every 8 h for the first 72 h to remove nonadherent cells. Isolation of the potential MSCs from the bone marrow exudate was accomplished by a two-step process on the basis of differential adherence of cells to the plastic (51). First, adherent cells were lifted with 0.1% trypsin for no more than 2 min. Lifted cells were removed, were replated into a new T-75 cm^2 with fresh media, and were allowed to reach approximately 70% confluence. The adherent population of cells was lifted again with 0.1% trypsin, was pelleted, and was resuspended in phosphate-buffered saline (PBS) for further isolation by use of commercially available stem cell isolation procedure (BD Biosciences) by treating the cell suspensions with biotinylated CD54 and CD90 antibodies followed by incubation of BD IMag streptavidin particles. Repeated washing of this mixture in the BD iMagnet permitted the isolation of antibody-purified populations of MSCs. Flow cytometry analysis was performed to verify that the selected cells expressed CD54 and CD90 and did not express the hematopoietic marker CD45 (see Figure SF1 of the Supporting Information).

Cell Transfection. rMSC cells were plated in optical dishes at 30 000 cells/cm^2 and were cultured at 37 °C with 5% CO_2 in Dulbecco's modified Eagle's medium (DMEM-7777) (Sigma) supplemented with addition of 10% fetal bovine serum (Hyclone) and 20 mM glutathione monoester. Cellular transfection by a single challenge of the NP-complex (6.6 pmol) was carried out 24 h after plating, and the media was exchanged after 24 h of transfection to remove any nontransfected NP-complex. Optical imaging of the transfected cells was carried out at 24 h post-transfection. Cell division occurred over the time span of the experiment, with a doubling rate of approximately 3 d.[75] Cell viability at 90% following transfection for all experiments was verified at 24 h using a Trypan blue exclusion test. No evidence of chromosomal condensation or change in cell morphology was observed following transfection indicative of no cytotoxicty at the transfection agent concentrations employed in this study. The MSCs were analyzed using selected surface marker analysis against control cells following the transfection step.

BDNF/mCherry Secretion Gene and eGFP Gene. The 6.6 kbp psec BDNF/mCherry fusion was prepared by linearizing a circular plasmid containing the cytomegalovirus (CMV) promoter and the c-DNA incorporating a psec-2 tag, brain-derived neurotrophic factor (BDNF) (ATCC), and mCherry (Clontech). The circular plasmid was prepared by the molecular cloning facility at Florida State University and was linearized (single cut site) by treatment with PCII nuclease New England Biolabs (NEB) following the manufacturer's protocol. The digested plasmid (single cut site) was analyzed on a 1% agarose gel to validate digestion. A synthetic dsDNA linker strand (35/39bp) containing a 4bp overhang and a protected 5′ C_6 thiol modification to the phosphate backbone was ligated to the linearized plasmid by standard T4 ligation methods (NEB) to allow appending to the AuNP surface. The ligated plasmid containing the chemically protected C_6 thiol spacer was precipitated by addition of EtOH and was stored at 4 °C. The sequences are available in Table 1 of the Supporting Information. In the linearized gene, the BDNF coding region precedes the mCherry coding region to allow mCherry cellular fluorescence to be an optical probe of the transcribed fusion protein.

The eGFP was prepared similarly to the psec-BDNF/mCherry plasmid; the only notable changes are the digestion enzyme (SPEI) and the appropriate 39mer linker (CATG overhang).

Ku70 AuNP-Gene Construct. The AuNP-complex was prepared by coassembly of Ku70 and a linker-modified (gene) in a 50:1 ratio via sequential thiol place exchange reactions. Prior to appending to the AuNP surface, the synthetically modified linearized plasmid was deprotected by treatment with dithiothreitol (DTT) and was purified by passing through a NAP-5 (Sephadex G-25 DNA grade) gravity flow size exclusion column following the manufacturer's protocol. Isolation of the linearized DNA was verified by UV−vis analysis of the 260 nm absorption for DNA. The deprotected plasmid was reactive toward disulfide formation (stable for ∼30 min at RT), and therefore, the gene was immediately used. Appending the plasmid to the AuNP was accomplished by a place exchange reaction using a 1.1:1 plasmid to AuNP ratio for 48 h resulting in formation of a AuNP−sulfur bond between the gene and the AuNP surface. The assembled AuNP-gene was pelleted out by centrifugation at 3000 rpm to remove unbound plasmid. Co-assembly of Ku70 onto the AuNP-gene construct was accomplished in a second place exchange reaction following the protocol described previously to dual label a AuNP with separate nucleic acid sequences.[46] The assembled AuNP-complex was isolated by pelleting at 3000 rpm and was stored at −20 °C.

Ku70 CdSe/ZnS Core@Shell (Ku70 QD_{gfs}488). Spherical 6.0 nm CdSe/ZnS shelled quantum dots (QD_{gfs}488) were prepared via literature protocols using a two-step SILAR protocol on the basis of CdO/TOPSe for preparation of the core and dimethylzinc/TMS-S for shelling. Briefly, the CdSe core was prepared by adding CdO (5.8 mg, 0.125 mmol), octadecylphosphonic acid (ODPA) (83.5 mg, 0.25 mmol), and 6 mL 1-octadecene into a three-neck round-bottom flask heated to 300 °C under N_2 flow until the solution was clear. The reaction was cooled to 220 °C prior to CdSe core formation, which was accomplished by rapid injection of 1 mL of 1 M trioctyl phosphine (TOP)Se, reaction at 220 °C for 10 min, followed by reaction at 150 °C for 8 h. The CdSe cores were isolated from unreacted materials by centrifugation prior to shelling through addition of toluene followed by MeOH to initiate precipitation.

Shelling the CdSe core by two monolayers of ZnS was accomplished by redissolving the CdSe cores into hexadecylamine (HDA) at 180 °C, alternating addition of dimethylzinc in TOP (0.32 M) and bis(trimethylsilyl)sulfide in TOP (0.28 M). The CdSe/ZnS core−shell was passivated by the N-terminus cysteine modified Ku70 using phase transfer from tetrachloroethylene (TCE) to water in the

dx.doi.org/10.1021/ja505190q | J. Am. Chem. Soc. 2014, 136, 14763−14771

presence of Ku70 at 60 °C. The exchange protocol was carried out in N_2 sparged, aqueous solution (2 mL) containing 2 M peptide and 0.05 mM of TCEP. The solution was stirred for 10 min, tetraethylammonium hydroxide (20 wt %) in diH_2O was added dropwise to achieve a pH of 10.0, and the mixture was allowed to phase separate. The water-solubilized fraction was removed, and Ku70 $QD_{gfs}488$ was isolated by EtOH precipitation (two times). Ku70 $QD_{gfs}488$ was resuspended in 0.2 μM filtered H_2O for storage at 4 °C.

RESULTS

Assembly of Ku70 Nanoparticle Complexes. The nanoparticle complex in Figure 1 represents the Ku70 AuNP-gene construct that incorporates a linearized gene to induce expression of a secreting BDNF/mCherry fusion protein and the pentapeptide N-cys-Ku70 peptide to induce rMSC uptake of the transfection package. The Ku70 peptide is designed from Bax inhibiting peptides (BIP) with a zwitterionic charge when the cysteine is bound to the AuNP surface.[72] The zwitterionic pentapeptide, N-termini cys-Ku-70 Bax-binding domain (PMLKE), is a known membrane permeable peptide that has an isoelectric point of 6.18 to minimize unwanted electrostatic interactions between the gene and AuNP peptide surface.[72] The gene (Figure 1B) contains a secretory tag (p-sec), CMV promoter, and the cDNA encoding for the BDNF/mCherry fusion. The BDNF/mCherry gene allows direct verification of transfection by observing protein expression through visualization of the mCherry fluorescence in live-cell microscopy experiments. The p-sec tag allows the protein to be secreted, which is important for downstream cell therapeutic biomedical applications.

The AuNP-complex in Figure 1A is assembled stepwise by first appending the C_6-thiol functionalized 6.6 kbp linearized plasmid through place exchange of citrate-passivating groups on a 6.6 nm AuNP surface. The cysteine modified Ku70 (N-cys-Ku70) peptide is assembled in a second place exchange reaction. The second place exchange reaction is often termed back-loading which is routinely employed for manipulating stoichiometry of passivants at AuNP surfaces or on Au thin films where the passivating moieties have dramatically different diffusion behavior.[76,77] The N-terminal cysteine coordinates through a bidentate coordination of the peptide to the AuNP surface, while the gene is bound through a monodentate Au-thiol linkage, which is cleaved with a half-life of 6 h in endosomal environments, on the basis of earlier studies.[46]

Confirmation of complex formation following the second place exchange reaction is provided by the AuNP localized surface plasmon resonance (LSPR) shift from 525 nm in 6.6 nm citrate passivated gold to 545 nm in the NP-complex as shown in Figure SF2 of the Supporting Information.[78−80] The LSPR frequency for 6.6 nm AuNP has been reported to be between 519 and 525 nm.[80] The red shift upon place exchange of the phosphine by a cysteine on the peptide produces the red shift in LSPR and will be loading level and AuNP size dependent.[81,82]

The DLS data for the AuNP-complex shows hydrodynamic radii of 133 nm, assuming a globular conformation. The AuNP with the gene appended and BSPP as the ligand is 130 nm. In comparison, the DLS measured hydrodynamic size for the BSPP passivated AuNP is 15 nm, while the gene alone is 97 nm. The observation of the AuNP being 2 times the expected size has been reported by Oh et al.[83] The BSPP is ~0.7 nm on the basis of calculations from [Au-(P-$(ph)_3)_3$] X-ray diffraction (XRD) structures. The DLS size of 15 nm for the BSPP passivated AuNP therefore is reasonable if we assume ~7 nm for the AuNP and 1.4 nm for the BSPP passivation (reflecting 2 times the BSPP size). The size difference for the AuNP core in transmission electron microscopy (TEM) versus DLS likely reflects salts, waters of solvation, and artifacts associated with DLS for a AuNP.

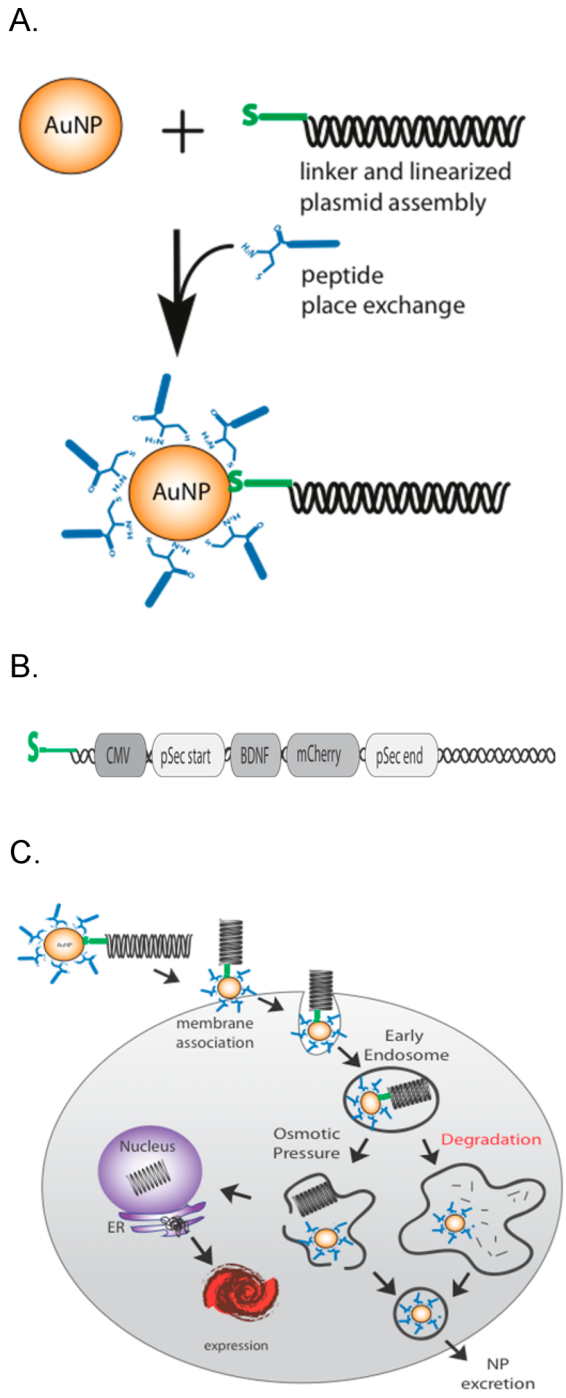

Figure 1. (A) Assembly of the AuNP-complex. (B) The 6.6 kbp fusion gene. (C) Schematic of cellular uptake of the AuNP-complex and subsequent exogenous BDNF/mCherry protein expression.

Consistent with assembly of the AuNP-complex, the hydrodynamic radius increases following the place exchange reactions. When assembled onto the AuNP, we expect the size increase to reflect the combination of the AuNP and the gene, but a compaction can arise because of electrostatic and van der

dx.doi.org/10.1021/ja505190q | J. Am. Chem. Soc. 2014, 136, 14763−14771

Waal forces. In the DLS data, the increase in size from 130 to 133 nm when the protein transduction domain (PTD) displaces the BSPP is consistent with the replacement of BSPP by the peptide (expected size 2.1 nm for one PTD vs BSPP at ∼0.7 nm) and roughly can be calculated by considering the AuNP plus PTD.

The increase in hydrodynamic ratio for the AuNP-complex supports the proposed assembly. DLS measurements were not performed on the $QD_{gfs}488$ because of instrumental design limitations and because of the minimal size change that would occur when the nanoparticles are modified only by the peptides.

Quantification of the peptide to gene on the AuNP is accomplished by analyzing the AuNP-complex by UV−vis absorption spectroscopy analysis coupled to cyanide digestion of the AuNP. In Figure 2A, the absorption spectra for the AuNP-complex is shown before (solid line) and after (dashed) cyanide treatment. In Figure 2A, the absorption feature at 545 nm is assignable to the AuNP localized surface plasmon resonance (LSPR); the feature at 260 nm is attributed to absorption by the nucleic acid residues of the gene, and the shoulder at 280 nm arises from the Cys amino acid residue on the peptide. The 6.6 kbp gene dominates the absorption between 260 and 280 nm, allowing the ratio of the gene to AuNP to be estimated at 1:1 gene to AuNP prior to cyanide digestion. Confirmation of the estimate is provided in Figure SF3 of the Supporting Information for the AuNP-gene construct without the peptide, where a 1:1 ratio is confirmed by absorption intensities. The gene-to-peptide ratio is calculated by the AuNP to allow the 260/280 nm ratio to be evaluated by fitting the absorption profile in the inset of Figure 2A.

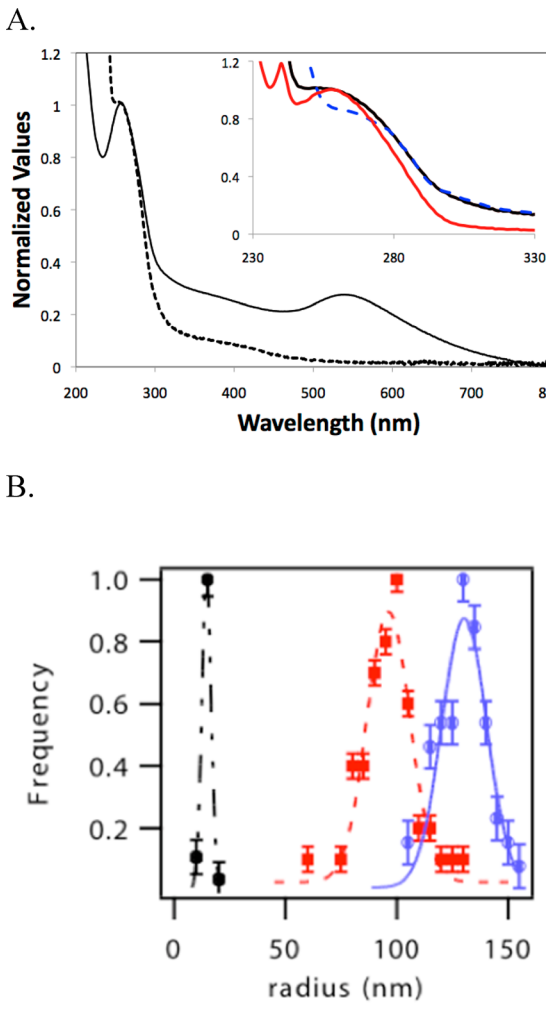

Figure 2. (A) Absorption spectra of AuNP-complex before (solid) and after (dashed) cyanide digestion. The inset shows the absorption shift for the AuNP-complex (black) and the AuNP complex lacking Ku70 (red) compared to uncomplexed Ku70 (blue). (B) Dynamic light scattering data for the AuNP-gene (blue, 130 nm), the linearized gene (red, 97 nm), and a 6.6 nm water-soluble BSPP-AuNP (black, 15 nm).

By analyzing the intensity ratios using the extinction coefficient for the gene and peptide, the coassembly process yields a single gene per AuNP and ∼500 N-cys-Ku70 peptides on the surface of a 6.6 nm AuNP core. The actual peptide and gene-loading levels reflect ensemble averages and will be stochastic varying per particle, as demonstrated previously.[46] The number of substitutions on the AuNP is consistent with earlier studies for peptide modification of AuNP.[58,84] The details of the cyanide digestion procedure and absorption spectra calculation of gene to peptide to AuNP are provided in the Supporting Information. The absorption data for the Ku70 $QD_{gfs}488$ is shown in Figure SF4 of the Supporting Information. No calculations were performed to quantify the peptide to the $QD_{gfs}488$ loading ratios because of the inability to dissolve the core NP and the strongly overlapping absorption for the peptides and excitonic features of the QD in the UV region of the absorption data.

On the basis of the calculated loading level of peptide per AuNP, a value of 3.6 ligands/nm^2 is obtained. The loading efficiency to the surface of the gold nanoparticle for a small peptide is within the range of current reported literature values (1.8−6.4 ligands/nm^2).[77,84,85] The estimated footprint of the thiol binding is approximately 0.214 nm^2, and the peptide length itself is approximately 2.1 nm.[86]

Expression of BDNF/mCherry Secretion Following Single Pass Ku70 AuNP Assisted Gene Transfection. Gene expression following a single transfection requires cytosolic escape and nuclear transcription for BDNF/mCherry expression (Figure 1C). Because the AuNP-complex is designed as a 6.6 kbp fusion gene, mCherry expression can only be observed if BDNF has already been transcribed. The use of the fusion gene allows the use of live-cell optical microscopy to observe the efficiency of transfection by monitoring the protein expression of mCherry directly and by monitoring the expression of BDNF in the rMSCs by inference. The optical images in Figure 3 show clear evidence of mCherry expression within the rMSCs. Analysis of the optical image provides a qualitative analysis of the transfection yield with >80% of the rMSC cells expressing within 4 days of transfection by the AuNP-complex. To establish that the transfection of the gene is not unique to the 6.6 kbp BDNF/mCheery sequence, we observed efficient transfection of a 4.8 kbp eGFP gene on the 6.6 nm AuNP passivated by Ku70 with subsequent expression of eGFP within rMSC cells as demonstrated by optical microscopy (Figure SF6 of the Supporting Information).

Evidence of the time-dependent evolution of the secreted BDNF/mCherry fusion protein in the media is provided by semiquantitative Western blot analysis of trichloroacetic acid precipitation of the media. Antibody staining of the Western reveals the presence of both BDNF and mCherry secreted into the media 15 days post-transfection (Figure 4A). Inspection of

dx.doi.org/10.1021/ja505190q | J. Am. Chem. Soc. 2014, 136, 14763−14771

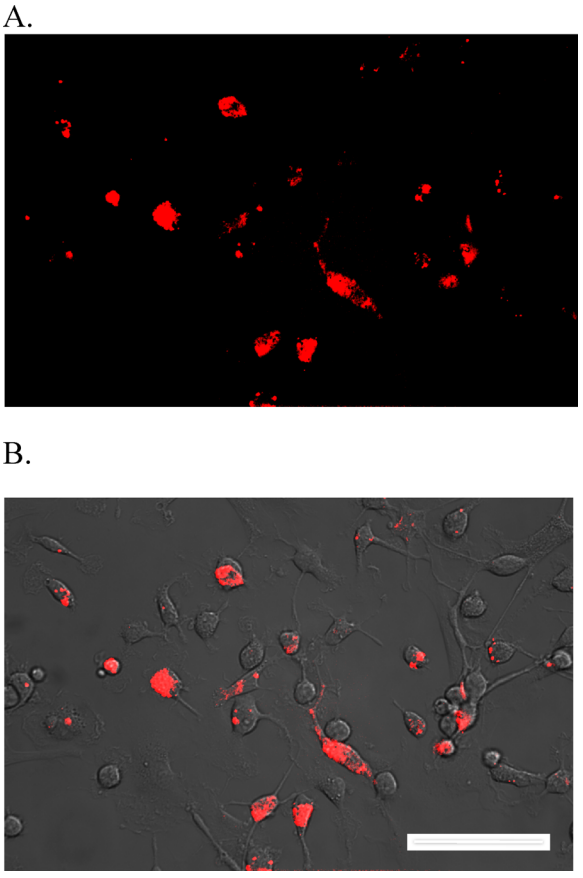

Figure 3. Wide-field optical imaging 4 d post-transfection of rMSC by AuNP-complex (A) monitored in the red channel (Texas Red) and (B) overlaid with the differential image contrast to allow the cell boundaries to be identified. The image indicates ~80% of cells exhibit mCherry expression at 4 d.

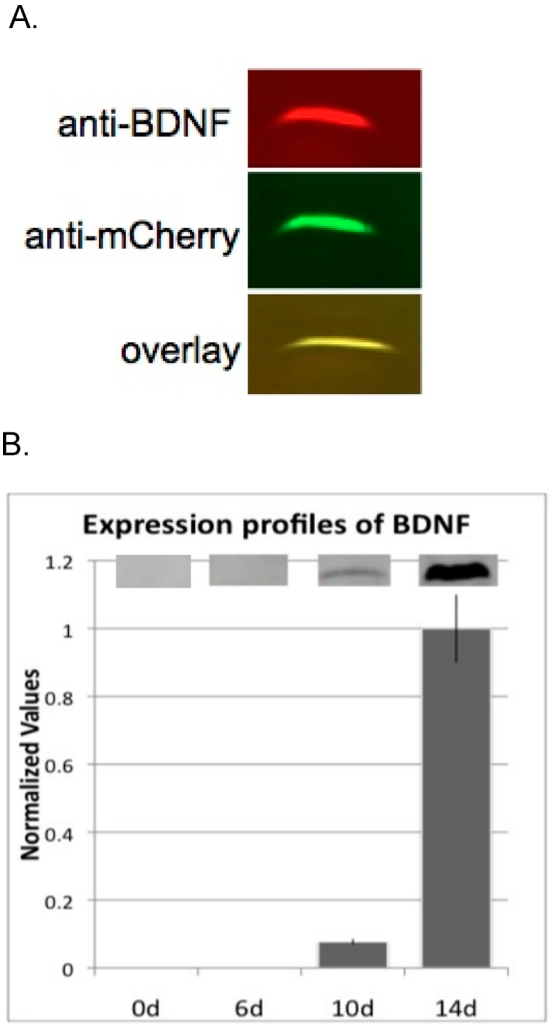

Figure 4. (A) Antibody staining of Western blot of the media at 15 d for mCherry, BDNF, and dual-stained slices indicating the presence of the desired protein. (B) Time-dependent secretion levels for BDNF expression using Western blot analysis of 2 mL media controlled against pretransfection levels. The plot is normalized to expression at 14 d. (Inset shows the densiometric analysis of the isolated bands from the Western blot.) A full gel is available in the Supporting Information.

the BDNF antibody stained gel at 0, 6, 10, and 14 d for identical media aliquots is shown in Figure 4B. Experimental levels out to 42 d and against a human BDNF and a protein ladder are shown in Figure SF5 of the Supporting Information. The rise in concentration of BDNF following transfection is controlled against the pretransfection BDNF levels. The delay in turn on of secreted BDNF in the Western blot (<10 d) compared to the optical imaging of mCherry (<4 d) reflects the imaging modality. The optical imaging is of cytosolic mCherry, while the Western blot images the BDNF and by supposition mCherry secreted into the media. Secretion into the media is diluted significantly limiting early time detection by Western blot methods.

Cell viability was assayed over the course of the 2 weeks and at 15 days post-transfection by trypan blue on a Cedex Cell Counter and Analyzer system, revealing that rMSC survival was 98 ± 3% after the single transfection, consistent with earlier reports of high cell viability following AuNP of no direct effect on the rMSC line as demonstrated by comparison of a limited number of surface markers for the transfected and non-transfected controls where no significant changes to the antibody markers for CD-90 (positive), CD-54 (positive), and CD-45 (negative) were observed indicative of maintenance of stem properties (Figure SF1 of the Supporting Information). The optical images clearly show evidence of fluorescent gene expression in <4 days, while the expression level by Western blot analysis of the media showed expression of the fusion product in approximately 10 days. These observations in conjunction with the surface marker analysis and viability assays provide direct evidence of successfully producing a genetically modified MSC population using the AuNP-complex for transfection with no apparent downstream effects on the MSCs.

Comparison of Ku70 AuNP Enhanced Transfection to Traditional Transfection Approaches in rMSCs. It is well-established that transfecting MSCs using nonviral approaches is poor, where typical reported values for single-pass transfection of MSCs are ~50% for Nucleofector[28−31] and 2−35% for cationic liposomes.[38−43] The transfection performance as measured by mCherry expression for delivery of equamolar concentrations of the BDNF/mCherry fusion gene using Lipofectamine$_{2000}$ is compared to Ku70 AuNP mediated transfection by analysis of wide-field microscopy analysis (10×) in the red channel. The optical images are available in the Supporting Information and indicate that transfection efficiencies for Lipofectamine$_{2000}$ are <1% for the rMSCs compared to >80% expression in the Ku70 assisted transfection.

dx.doi.org/10.1021/ja505190q | J. Am. Chem. Soc. 2014, 136, 14763−14771

No uptake was observable for exposure of the AuNP-gene without Ku70 (data not shown).

Ku70 Assisted Transfection When Appended to QDs. The effectiveness of Ku70 to enhance transfection efficiencies in AuNPs can be shown to be generalizable to core@shell quantum dots ($QD_{gfs}488$). The $QD_{gfs}488$ are spherical and have <5% size dispersity. The photoluminescence emission is centered at 488 nm with a full width at half-maximum of 24 nm. The Ku70 loading level on the nanoparticles is maintained at 10% of the available sites by utilizing a control peptide (CAAKA) to allow approximate correlation with the gene studies since the appended 6.6 kbp gene is believed to occupy part of the AuNP surface.

The Ku70 $QD_{gfs}488$ nanoparticles are transfected at 3 μM for 30% confluent rMSCs. Uptake analysis of the wide-field images indicates that 82% of the cells are transfected following treatment. In Figure 5, confocal field microscopy images reveal QD uptake within 24 h with localization of the transfected packages via endosomal encapsulation on the basis of Z-stack imaging. In the Z-stack, the cells are stained with a nucleus stain, 4',6-diamidino-2-phenylindole (DAPI), and a surface stain, and wheat germ agglutinin of 594 nm is used to verify internalization and no surface association. No experimental evidence of cell membrane association or cell membrane penetration can be observed, but following transfection, the Ku70-$QD_{gfs}488$ is observed surrounding the nucleus, as shown in the DIC overlay (Figure 5). The QD is observed to be present in the rMSC 5 d post-transfection (Figure 5). The results of the Ku70 modified QD and AuNP confirm that improved transfection yields are achievable for rMSCs following a single treatment by use of a Ku70 zwitterionic CPP nanoparticle surface appendage to enhance cellular internalization.

CONCLUSION

The results of this study establish a novel methodology to transfect MSCs using Ku70 as a transfection agent of nanoparticles, whether a AuNP or a CdSe/ZnS core@shell quantum dot. The use of the AuNP comodified by a gene and the Ku70 peptide is shown to effectively alter protein expression in MSCs and illustrates that gene transfer on a AuNP peptide fusion can induce an efficient one-step transformation of rMSCs. The Ku70 modified nanoparticles are believed to utilize the natural cellular uptake without affecting cell viability. The alteration of protein expression within the rMSC following transfection and endosomal escape of the gene results in an enriched rMSC population in a single transfection step, while avoiding viral methods, electroporation strategies, or commercial lipids that can invoke an apoptotic response. While the methods are adaptable to other nanoparticles, the use of AuNPs to genetically alter rMSCs is potentially transformative for generating therapeutic cell lines, since gold is FDA approved for preclinical trials.

The study confirms that when the Ku70 AuNP gene construct is transfected into the rMSC, 80% of the treated MSCs exhibit the desired protein expression within 4 days indicating that a therapeutic cell line could be generated from this NP-complex treatment. The results offer a simple efficient approach to transfection without complication from viral methods. The ability to isolate a genetically altered MSC line that exhibits no loss in viability and exhibits no significant impact on AB markers compared to the controls within 4 days of treatment is an important step toward being able to isolate a genetically modified stem cell for cell therapy applications. The combination of being able to selectively engineer the NP and the delivered gene is an innovative strategy that will allow rapid translation of this novel class of materials for biomedical applications.

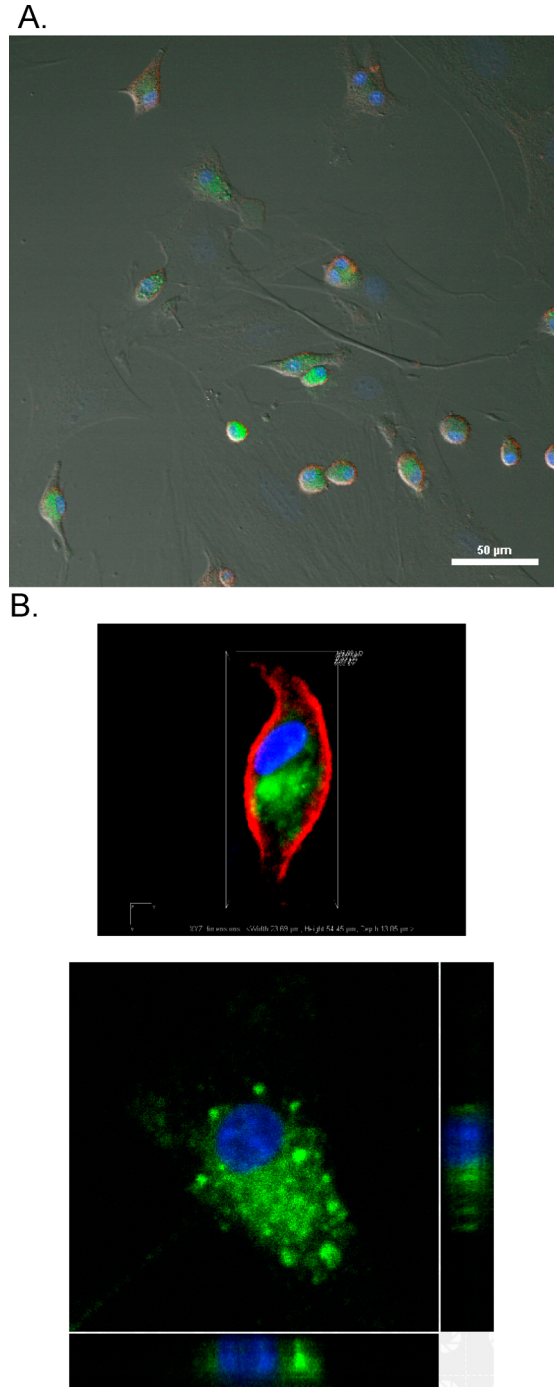

Figure 5. (A) Optical image with $QD_{gfs}488$ as green, wheat germ agglutinin (WGA) 594 nm for a membrane stain, and a blue DAPI nuclei stain. The proximity of the $QD_{gfs}488$ is within the cell 5 d post-transfection (40×). (B) 3D images 5 d post-transfection with $QD_{gfs}488$ within the rMSCs that demonstrates internalized $QD_{gfs}488$.

dx.doi.org/10.1021/ja505190q | J. Am. Chem. Soc. 2014, 136, 14763−14771

■ ASSOCIATED CONTENT

Supporting Information

Absorption and digestion data for calculating the peptide:gene:AuNP ratios, flow cytometry analysis of a surface markers for the MSC, and optical results for lipofectamine transfection. This material is available free of charge via the Internet at http://pubs.acs.org.

■ AUTHOR INFORMATION

Corresponding Author

Strouse@chem.fsu.edu

Author Contributions

[§]These authors contributed equally.

Notes

The authors declare no competing financial interest.

■ ACKNOWLEDGMENTS

We wish to acknowledge the National Science Foundation under CHE-0911080 for support of the research as well as the Florida State University Office of Research Planning grant CRC-PG 075000-140.

■ REFERENCES

(1) Santos, J. L.; Pandita, D.; Rodrigues, J.; Pego, A. P.; Granja, P. L.; Tomas, H. *Curr. Gene Ther.* **2011**, *11*, 46.

(2) Scheibe, F.; Gladow, N.; Mergenthaler, P.; Tucker, A. H.; Meisel, A.; Prockop, D. J.; Priller, J. *Gene Ther.* **2012**, *19*, 550.

(3) Ferreira, E.; Potier, E.; Logeart-Avramoglou, D.; Salomskaite-Davalgiene, S.; Mir, L. M.; Petite, H. *Gene Ther.* **2008**, *15*, 537.

(4) Abdallah, B. M.; Kassem, M. *Gene Ther.* **2008**, *15*, 109.

(5) Chen, J.; Li, Y.; Katakowski, M.; Chen, X.; Wang, L.; Lu, D.; Lu, M.; Gautam, S. C.; Chopp, M. *J. Neurosci. Res.* **2003**, *73*, 778.

(6) Sokolova, I. B.; Fedotova, O. R.; Tsikunov, S. G.; Polyntsev, D. G. *Bull. Exp. Biol. Med.* **2011**, *151*, 130.

(7) Bernstein, H. S.; Srivastava, D. *Pediatr. Res.* **2012**, *71*, 491.

(8) Joyce, N.; Annett, G.; Wirthlin, L.; Olson, S.; Bauer, G.; Nolta, J. A. *Regener. Med.* **2010**, *5*, 933.

(9) Reagan, M. R.; Kaplan, D. L. *Stem Cells* **2011**, *29*, 920.

(10) Ren, G.; Chen, X.; Dong, F.; Li, W.; Ren, X.; Zhang, Y.; Shi, Y. *Stem Cells Transl. Med.* **2012**, *1*, 51.

(11) Samper, E.; Diez-Juan, A.; Montero, J. A.; Sepulveda, P. *Stem Cell Rev.* **2013**, *9* (3), 266−280.

(12) Shah, K. *Adv. Drug Delivery Rev.* **2012**, *64*, 739.

(13) Honmou, O.; Onodera, R.; Sasaki, M.; Waxman, S. G.; Kocsis, J. D. *Trends Mol. Med.* **2012**, *18*, 292.

(14) Sykova, E.; Jendelova, P. *Prog. Brain Res.* **2007**, *161*, 367.

(15) Yi, T.; Song, S. U. *Arch. Pharm. Res.* **2012**, *35*, 213.

(16) Hamm, A.; Krott, N.; Breibach, I.; Blindt, R.; Bosserhoff, A. *Tissue Eng.* **2002**, *8*, 235.

(17) Madeira, C.; Mendes, R. D.; Ribeiro, S. C.; Boura, J. S.; Aires-Barros, M. R.; da Silva, C. L.; Cabral, J. M. *J. Biomed. Biotechnol.* **2010**, *2010*, 735349.

(18) Gandra, N.; Wang, D. D.; Zhu, Y.; Mao, C. *Angew. Chem., Int. Ed.* **2013**, *52*, 11278.

(19) Choi, H. S.; Frangioni, J. V. *Mol. Imaging* **2010**, *9*, 291.

(20) Greco, S. J.; Rameshwar, P. *Ther. Delivery* **2012**, *3*, 997.

(21) Trounson, A. *BMC Med.* **2009**, *7*, 29.

(22) Glover, D. J.; Lipps, H. J.; Jans, D. A. *Nat. Rev. Genet.* **2005**, *6*, 299.

(23) Jang, J. H.; Schaffer, D. V.; Shea, L. D. *Mol. Ther.* **2011**, *19*, 1407.

(24) Liu, F.; Huang, L. *J. Controlled Release* **2002**, *78*, 259.

(25) Mansouri, S.; Lavigne, P.; Corsi, K.; Benderdour, M.; Beaumont, E.; Fernandes, J. C. *Eur. J. Pharm. Biopharm.: Official Journal of Arbeitsgemeinschaft fur Pharmazeutische Verfahrenstechnik e.V* **2004**, *57*, 1.

(26) Park, J. S.; Na, K.; Woo, D. G.; Yang, H. N.; Kim, J. M.; Kim, J. H.; Chung, H. M.; Park, K. H. *Biomaterials* **2010**, *31*, 124.

(27) Pouton, C. W.; Seymour, L. W. *Adv. Drug Delivery Rev.* **2001**, *46*, 187.

(28) Aluigi, M.; Fogli, M.; Curti, A.; Isidori, A.; Gruppioni, E.; Chiodoni, C.; Colombo, M. P.; Versura, P.; D'Errico-Grigioni, A.; Ferri, E.; Baccarani, M.; Lemoli, R. M. *Stem Cells* **2006**, *24*, 454.

(29) Peister, A.; Mellad, J. A.; Wang, M.; Tucker, H. A.; Prockop, D. J. *Gene Ther.* **2004**, *11*, 224.

(30) Gresch, O.; Altrogge, L. *Methods Mol. Biol.* **2012**, *801*, 65.

(31) Flanagan, M.; Gimble, J. M.; Yu, G.; Wu, X.; Xia, X.; Hu, J.; Yao, S.; Li, S. *Cancer Gene Ther.* **2011**, *18*, 579.

(32) Silva, F. H.; Nardi, N. B. *Med. Hypotheses* **2006**, *67*, 922.

(33) Seth, P. *Cancer Biol. Ther.* **2005**, *4*, 512.

(34) Locke, M.; Ussher, J. E.; Mistry, R.; Taylor, J. A.; Dunbar, P. R. *Tissue Eng., Part C: Methods* **2011**, *17*, 949.

(35) Choudhary, S.; Marquez, M.; Alencastro, F.; Spors, F.; Zhao, Y.; Tiwari, V. *J. Biomed. Biotechnol.* **2011**, *2011*, 264350.

(36) Chen, C. Y.; Wu, H. H.; Chen, C. P.; Chern, S. R.; Hwang, S. M.; Huang, S. F.; Lo, W. H.; Chen, G. Y.; Hu, Y. C. *Mol. Pharmaceutics* **2011**, *8*, 1505.

(37) Thomas, C. E.; Ehrhardt, A.; Kay, M. A. *Nat. Rev. Genet.* **2003**, *4*, 346.

(38) Ye, Z.; Yu, X.; Cheng, L. *Methods Mol. Biol.* **2008**, *430*, 243.

(39) Zeng, J.; Du, J.; Zhao, Y.; Palanisamy, N.; Wang, S. *Stem Cells* **2007**, *25*, 1055.

(40) Liew, C. G.; Draper, J. S.; Walsh, J.; Moore, H.; Andrews, P. W. *Stem Cells* **2007**, *25*, 1521.

(41) Barrow, K. M.; Perez-Campo, F. M.; Ward, C. M. *Methods Mol. Biol.* **2006**, *329*, 283.

(42) Kim, J. H.; Do, H. J.; Choi, S. J.; Cho, H. J.; Park, K. H.; Yang, H. M.; Lee, S. H.; Kim, D. K.; Kwack, K.; Oh, S. K.; Moon, S. Y.; Cha, K. Y.; Chung, H. M. *Exp. Mol. Med.* **2005**, *37*, 36.

(43) Lei, Y.; Tang, H.; Yao, L.; Yu, R.; Feng, M.; Zou, B. *Bioconjugate Chem.* **2008**, *19*, 421.

(44) Peng, L. H.; Fung, K. P.; Leung, P. C.; Gao, J. Q. *Drug Discovery Today* **2011**, *16*, 957.

(45) Aronovich, E. L.; McIvor, R. S.; Hackett, P. B. *Hum. Mol. Genet.* **2011**, *20*, R14.

(46) Muroski, M. E.; Kogot, J. M.; Strouse, G. F. *J. Am. Chem. Soc.* **2012**, *134*, 19722.

(47) Albanese, A.; Chan, W. C. *ACS Nano* **2011**, *5*, 5478.

(48) Chen, L. Q.; Xiao, S. J.; Hu, P. P.; Peng, L.; Ma, J.; Luo, L. F.; Li, Y. F.; Huang, C. Z. *Anal. Chem.* **2012**, *84*, 3099.

(49) Chithrani, B. D.; Ghazani, A. A.; Chan, W. C. W. *Nano Lett.* **2006**, *6*, 662.

(50) Deng, D.; Zhang, D.; Li, Y.; Achilefu, S.; Gu, Y. *Biosens. Bioelectron.* **2013**, *49*, 216.

(51) Guo, S.; Huang, Y.; Jiang, Q.; Sun, Y.; Deng, L.; Liang, Z.; Du, Q.; Xing, J.; Zhao, Y.; Wang, P. C.; Dong, A.; Liang, X. J. *ACS Nano* **2010**, *4*, 5505.

(52) Hong, R.; Han, G.; Fernández, J. M.; Kim, B. J.; Forbes, N. S.; Rotello, V. M. *J. Am. Chem. Soc.* **2006**, *128*, 1078.

(53) Kawano, T.; Yamagata, M.; Takahashi, H.; Niidome, Y.; Yamada, S.; Katayama, Y.; Niidome, T. *J. Controlled Release* **2006**, *111*, 382.

(54) Leu, J. G.; Chen, S. A.; Chen, H. M.; Wu, W. M.; Hung, C. F.; Yao, Y. D.; Tu, C. S.; Liang, Y. J. *Nanomed.: Nanotechnol., Biol., Med.* **2012**, *8*, 767.

(55) Murphy, C. J.; Gole, A. M.; Stone, J. W.; Sisco, P. N.; Alkilany, A. M.; Goldsmith, E. C.; Baxter, S. C. *Acc. Chem. Res.* **2008**, *41*, 1721.

(56) Sandhu, K. K.; McIntosh, C. M.; Simard, J. M.; Smith, S. W.; Rotello, V. M. *Bioconjugate Chem.* **2002**, *13*, 3.

(57) Zhu, Z. J.; Tang, R.; Yeh, Y. C.; Miranda, O. R.; Rotello, V. M.; Vachet, R. W. *Anal. Chem.* **2012**, *84*, 4321.

(58) Rosi, N. L.; Giljohann, D. A.; Thaxton, C. S.; Lytton-Jean, A. K.; Han, M. S.; Mirkin, C. A. *Science* **2006**, *312*, 1027.

(59) Seferos, D. S.; Giljohann, D. A.; Hill, H. D.; Prigodich, A. E.; Mirkin, C. A. *J. Am. Chem. Soc.* **2007**, *129*, 15477.

(60) Giljohann, D.; Seferos, D.; Prigodich, A.; Patel, P.; Mirkin, C. *J. Am. Chem. Soc.* **2009**, *131*, 2072.
(61) Lee, J. S.; Green, J. J.; Love, K. T.; Sunshine, J.; Langer, R.; Anderson, D. G. *Nano Lett.* **2009**, *9*, 2402.
(62) Chugh, A.; Eudes, F.; Shim, Y. S. *IUBMB Life* **2010**, *62*, 183.
(63) Drin, G.; Cottin, S.; Blanc, E.; Rees, A. R.; Temsamani, J. *J. Biol. Chem.* **2003**, *278*, 31192.
(64) Fang, B.; Jiang, L.; Zhang, M.; Ren, F. Z. *Biochimie* **2013**, *95* (2), 251−257.
(65) Foerg, C.; Ziegler, U.; Fernandez-Carneado, J.; Giralt, E.; Rennert, R.; Beck-Sickinger, A. G.; Merkle, H. P. *Biochemistry* **2005**, *44*, 72.
(66) Fonseca, S. B.; Pereira, M. P.; Kelley, S. O. *Adv. Drug Delivery Rev.* **2009**, *61*, 953.
(67) Meade, B. R.; Dowdy, S. F. *Adv. Drug Delivery Rev.* **2007**, *59*, 134.
(68) Moschos, S. A.; Jones, S. W.; Perry, M. M.; Williams, A. E.; Erjefalt, J. S.; Turner, J. J.; Barnes, P. J.; Sproat, B. S.; Gait, M. J.; Lindsay, M. A. *Bioconjugate Chem.* **2007**, *18*, 1450.
(69) Richard, J. P.; Melikov, K.; Vives, E.; Ramos, C.; Verbeure, B.; Gait, M. J.; Chernomordik, L. V.; Lebleu, B. *J. Biol. Chem.* **2003**, *278*, 585.
(70) Santra, S.; Yang, H.; Stanley, J. T.; Holloway, P. H.; Moudgil, B. M.; Walter, G.; Mericle, R. A. *Chem. Commun. (Cambridge, U.K.)* **2005**, 3144.
(71) Song, H. P.; Yang, J. Y.; Lo, S. L.; Wang, Y.; Fan, W. M.; Tang, X. S.; Xue, J. M.; Wang, S. *Biomaterials* **2010**, *31*, 769.
(72) Gomez, J. A.; Gama, V.; Yoshida, T.; Sun, W.; Hayes, P.; Leskov, K.; Boothman, D.; Matsuyama, S. *Biochem. Soc. Trans.* **2007**, *35*, 797.
(73) Wuelfing, W.; Gross, S.; Miles, D.; Murray, R. *J. Am. Chem. Soc.* **1998**, *120*, 12696.
(74) Nadri, S.; Soleimani, M.; Hosseni, R. H.; Massumi, M.; Atashi, A.; Izadpanah, R. *Int. J. Dev. Biol.* **2007**, *51*, 723.
(75) Tawonsawatruk, T.; Spadaccino, A.; Murray, I. R.; Peault, B.; Simpson, H. A. *J. Med. Assoc. Thailand* **2012**, *95* (Suppl10), S189.
(76) Chompoosor, A.; Han, G.; Rotello, V. M. *Bioconjugate Chem.* **2008**, *19*, 1342.
(77) Woehrle, G. H.; Brown, L. O.; Hutchison, J. E. *J. Am. Chem. Soc.* **2005**, *127*, 2172.
(78) Haes, A.; Haynes, C.; McFarland, A.; Schatz, G.; Van Duyne, R.; Zou, S. *MRS Bull.* **2005**, *30*, 368.
(79) Cumberland, S.; Strouse, G. *Langmuir* **2002**, *18*, 269.
(80) Jain, P.; Qian, W.; El-Sayed, M. *J. Am. Chem. Soc.* **2006**, *128*, 2426.
(81) Breshike, C.; Riskowski, R.; Strouse, G. *J. Phys. Chem. C* **2013**, *117*, 23942.
(82) Kelly, K.; Coronado, E.; Zhao, L.; Schatz, G. *J. Phys. Chem. B* **2003**, *107*, 668.
(83) Oh, E.; Susumu, K.; Goswami, R.; Mattoussi, H. *Langmuir* **2010**, *26*, 7604.
(84) Kogot, J. M.; England, H. J.; Strouse, G. F.; Logan, T. M. *J. Am. Chem. Soc.* **2008**, *130*, 16156.
(85) Levy, R.; Thanh, N.; Doty, R.; Hussain, I.; Nichols, R.; Schiffrin, D.; Brust, M.; Fernig, D. *J. Am. Chem. Soc.* **2004**, *126*, 10076.
(86) Hakkinen, H. *Nat. Chem.* **2012**, *4*, 443.